TITLE:

A machine learning classifier trained on cancer transcriptomes detects NF1 inactivation signal in glioblastoma

AUTHORS:

[*]Gregory P. Way[a,b], [*]Robert J. Allaway[c], Stephanie J. Bouley[c], Camilo E. Fadul[d], Yolanda Sanchez[c,e,1], Casey S. Greene[b,2]

[*]these authors contributed equally to this work

AFFILIATIONS:

[a]Genomics and Computational Biology Graduate Program, University of Pennsylvania, Philadelphia, PA, USA

[b]Department of Systems Pharmacology and Translational Therapeutics, University of Pennsylvania, Philadelphia, PA, USA

[c]Department of Molecular and Systems Biology, Geisel School of Medicine at Dartmouth, Dartmouth College, Hanover, NH, USA.

[d]Department of Neurology, University of Virginia, Charlottesville, VA, USA

[e]Norris Cotton Cancer Center, Dartmouth-Hitchcock Medical Center, Lebanon, NH, USA

CO-CORRESPONDING AUTHORS:

[1]Geisel School of Medicine at Dartmouth, HB 7650, Hanover, NH 03755; Phone: 603-650-1669; Fax: 603-650-1669; yolanda.sanchez@dartmouth.edu

[2]10-131 SCTR 34th and Civic Center Blvd, Philadelphia, PA 19104; Phone: 215-573-2991; Fax: 215-573-9135; csgreene@upenn.edu

AUTHOR EMAILS:

GPW: gregway@mail.med.upenn.edu
RJA: Robert.J.Allaway.GR@dartmouth.edu
SJB: Stephanie.J.Bouley.GR@dartmouth.edu
CF: CEF3W@hscmail.mcc.virginia.edu
YS: Yolanda.Sanchez@dartmouth.edu
CSG: csgreene@mail.med.upenn.edu

KEYWORDS:

Neurofibromatosis Type I, Glioblastoma, Machine Learning, Cancer, NF1 Inactivation, Classifier

ABSTRACT (309/350):

Background

We have identified molecules that exhibit synthetic lethality in cells with loss of the neurofibromin 1 (*NF1*) tumor suppressor gene. However, recognizing tumors that have inactivation of the *NF1* tumor suppressor function is challenging because the loss may occur via mechanisms that do not involve mutation of the genomic locus. Degradation of the NF1 protein, independent of *NF1* mutation status, phenocopies inactivating mutations to drive tumors in human glioma cell lines. NF1 inactivation may alter the transcriptional landscape of a tumor and allow a machine learning classifier to detect which tumors will benefit from synthetic lethal molecules.

Results

We developed a strategy to predict tumors with low NF1 activity and hence tumors that may respond to treatments that target cells lacking NF1. Using RNAseq data from The Cancer Genome Atlas (TCGA), we trained an ensemble of 500 logistic regression classifiers that integrates mutation status with whole transcriptomes to predict NF1 inactivation in glioblastoma (GBM). On TCGA data, the classifier detected *NF1* mutated tumors (test set area under the receiver operating characteristic curve (AUROC) mean = 0.77, 95% quantile = 0.53 – 0.95) over 50 random initializations. On RNA-Seq data transformed into the space of gene expression microarrays, this method produced a classifier with similar performance (test set AUROC mean = 0.77, 95% quantile = 0.53 – 0.96). We applied our ensemble classifier trained on the transformed TCGA data to a microarray validation set of 12 samples with matched RNA and NF1 protein-level measurements. The classifier's NF1 score was associated with NF1 protein concentration in these samples.

Conclusions

We demonstrate that TCGA can be used to train accurate predictors of NF1 inactivation in GBM. The ensemble classifier performed well for samples with very high or very low NF1 protein concentrations but had mixed performance in samples with intermediate NF1 concentrations. Nevertheless, high-performing and validated predictors have the potential to be paired with targeted therapies and personalized medicine.

BACKGROUND:

Genomic tools allow investigators to devise therapies targeting specific molecular abnormalities in tumors. One such alteration is the loss of neurofibromin 1 (NF1), an important tumor suppressor that regulates the activity of *RAS* GTPases [1,2]. Heterozygous mutation or deletion of *NF1* causes neurofibromatosis type 1 (NF), one of the most frequently inherited genetic disorders [3]. NF patients often develop plexiform neurofibromas (PNs), benign nerve tumors for which the only therapy is surgery. However, resection is often impossible due to the tumor's intimate association with peripheral and cranial nerves [4]. PNs can transform to malignant peripheral nerve sheath tumors (MPNSTs), which are chemo- and radiation-resistant sarcomas with a dismal 20% 5-year survival [5]. In addition, patients with NF are susceptible to a broad spectrum of other tumors including low-grade/pilocytic astrocytomas, pheochromocytomas, optic nerve gliomas, and juvenile myelomonocytic leukemias [6]. Many aggressive non-NF associated (sporadic) tumors have recently been shown to harbor *NF1* mutations, including glioblastoma (GBM), neuroblastoma, melanoma, thyroid, ovarian, breast, and lung cancers [7]. Therefore, somatic and inherited loss of *NF1* function is emerging as a driver of tumors from different organ sites.

Several groups including our own have been working to develop therapeutic approaches to target tumors with loss of NF1. Previously, our lab developed a high throughput approach using yeast and mammalian screening platforms to identify tool compounds and drug targets for cancer cells in which

NF1 loss drives tumor formation. Our pipeline identified small molecules that selectively kill or stop the growth of MPNST cells carrying a mutation in *NF1* or yeast lacking the *NF1* homolog *IRA2* [8]. We also developed an assay in yeast to identify the targets of our lead tool compounds and found that one of these compounds (UC-1) shares a mechanism (phosphorylation of RNA Pol II CTD Ser2/5) with experimental drugs in clinical trials [8]. UC-1 impacts CTD phosphorylation, which is regulated by the CTD kinase Ctk1, the yeast homolog of human Cdk9. We showed that deletion of *CTK1* was synthetic lethal with loss of the yeast *NF1* homolog *IRA2*. Furthermore, we have found that inhibitors of this process (dinaciclib, SNS-032) can inhibit other types of RAS-dysregulated tumor cells [9].

However, relying on genetic data alone to identify tumors that may be susceptible to therapies targeting NF1 loss may leave a proportion of potentially actionable tumors unrecognized. NF1 tumor suppressor activity can be lost via mutation of the genomic locus, proteasome-mediated degradation, inhibition by miRNA, *de novo* insertion of an ALU element, and C→U editing of the *NF1* mRNA [10–14]. This complexity presents challenges when trying to identify tumors that will benefit from molecules that exert synthetic lethality with dysregulation of *NF1/RAS* pathways.

The Cancer Genome Atlas (TCGA) has released a large volume of data on several cancer tissues measured on a variety of genomic platforms. In the present study, we leverage TCGA GBM RNAseq expression data with matched mutation calls to construct a classifier capable of identifying an NF1 inactivation signature. This strategy sidesteps the problem of functional characterization of mutations by evaluating a regulator's downstream gene expression activity. We applied this signature to predict NF1 inactivation in a cohort of biobanked GBMs. In general, this approach can be translatable to any gene producing measurable downstream transcriptome-wide effects.

METHODS:

The Cancer Genome Atlas Data

120 We downloaded RNAseq and mutation data from TCGA Pan Cancer project from the UCSC Xena
121 data portal [15] and subset each dataset to only the GBMs [16]. The data consists of 607 GBMs; of which
122 291 have mutation calls, 172 have RNAseq measurements, and 149 have both RNAseq and mutation
123 calls. Of these 149 samples, 15 have inactivating *NF1* mutations (10.1%) and were used as gold standard
124 positives in building the classifier (Supplementary Table S1). Additionally, to reduce dimensionality while
125 avoiding unexpressed and invariant genes, we subset to the top 8,000 most variably expressed genes by
126 median absolute deviation. We z-scored all gene expression measurements. This resulted in final matrix
127 with dimension 149 samples by 8,000 genes. For use in platform independent predictions, we used
128 Training Distribution Matching (TDM) to transform the TCGA RNAseq data to match a microarray
129 expression distribution [17].
130
131 *Hyperparameter optimization*
132 Using the GBM RNAseq data, we trained logistic regression classifiers with an elastic net penalty
133 using stochastic gradient descent to detect tumors with NF1 inactivation. We identified high-performing
134 alpha and L1 mixing parameters using 5-fold cross validation ensuring balanced membership of *NF1*
135 mutations in each fold. Briefly, alpha controls how weight penalty and the L1 mixing parameter tunes
136 the amount of test set regularization by controlling the sparsity of the features. An L1 mixing parameter
137 value of zero corresponds to the L2 penalty and a value of one corresponds to the L1 penalty, with L1
138 bringing a sparser solution. We used python 3.5.1 and Sci-kit Learn for machine learning
139 implementations [18].
140
141 *Ensemble classifier construction and application to the validation set*

After selecting optimal hyperparameters, we constructed 500 classifiers that would compose our ensemble model. Specifically, across 100 different random initializations, we subset the full TCGA GBM data into 5 folds and trained a single classifier for each training fold.

We borrowed terminology from the epidemiology field to describe data partitioning. We trained our models on a "training" partition and assessed model performance on a "test" partition, which refers to the held out cross-validation fold. The independent "validation set" refers to the GBM dataset generated in a different lab (see Figure 1A).

Because of the small number of gold standard positive training examples, we were concerned about the stability of our model solutions. Therefore, we constructed an ensemble classifier from the 500 models. Specifically, we assigned each classifier a weight using the specific randomization's "test set" cross-validation AUROC. Lastly, for the final *NF1* inactivation prediction, we used the mean of the weighted predictions across all iterations as the *NF1* inactivation prediction. We applied this ensemble classifier to the validation set in which NF1 protein levels were directly measured.

Validation Sample Acquisition

Thirteen flash-frozen, de-identified GBM samples were obtained from the Maine Medical Center Biobank. Samples were received on dry ice and stored at -80°C until isolation of DNA/RNA/protein. To isolate DNA, tumor fragments of approximately 20 mg in mass were harvested on an aluminum block pre-chilled on dry ice. Samples were then immediately transferred to a mortar and pestle containing a small volume of liquid nitrogen. The fragments were pulverized in the mortar and pestle, and the liquid nitrogen was allowed to evaporate. Next, samples were immediately processed with a DNA/RNA/Protein Purification Plus kit (Norgen Biotek) following the standard operating protocol for animal tissue. DNA concentration and quality were assessed using an ND-1000 (Nanodrop), a Qubit Fluorometer (Thermo Scientific), and a Fragment Analyzer (Advanced Analytical Technologies). To

isolate RNA, -80 C tumor fragments were placed in 5-10 volumes of RNAlater-ICE Frozen Tissue Transition Solution (Ambion) and placed at -20°C until RNA extraction with a mirVana miRNA isolation kit, without phenol, following the standard operating protocol (Thermo Scientific). Samples were homogenized using a manual homogenizer in the presence of mirVana lysis buffer. RNA concentration and quality were determined using a Qubit Fluorometer (Thermo Scientific) and a Fragment Analyzer (Advanced Analytical Technologies). To isolate protein, small tumor fragments were pulverized and lysed in approximately 3 volumes of ice-cold radioimmunoprecipitation assay (RIPA) buffer (150 mM sodium chloride, 1% v/v nonidet P40, 0.5% w/v sodium deoxycholate, 0.05% w/v sodium dodecyl sulfate, 50 mM Tris pH 8.0) containing 1 mM sodium orthovanadate, 1 mM sodium fluoride, 1 mM phenylmethylsulfonyl fluoride, and 1X protease inhibitor cocktail (0.1 µg/mL leupeptin, 100 µM benzamidine HCl, 1 µM aprotinin, 0.1 µg/mL soybean trypsin inhibitor, 0.1 µg/mL pepstatin, 0.1 µg/mL antipain). Samples were passed through a 25 ⅝ g needle and subsequently sonicated on ice to promote efficient lysis and DNA shearing. After a 30 minute incubation on ice, lysates were cleared by centrifuging at 16100 x g for 20 minutes. HEK293T, U87-MG, and U87-MG cells treated with 1 micromolar bortezomib (Selleckchem) and 10 micromolar MG132 (Selleckchem) were also prepared in RIPA buffer. Protein samples were stored at -80°C until analysis.

RNA Microarray

After RNA isolation and QC, samples were labeled for the GeneChip Human Transcriptome Array 2.0 (HTA 2.0, Affymetrix). Labeling was performed with Affymetrix Proprietary DNA Label (biotin-linked) using a WT Plus Kit (Affymetrix) provided with the HTA 2.0, following the standard operating protocol for HTA 2.0, including PolyA controls. Hybridization, washing, and staining were performed with the WT Plus Kit, following the standard operating protocol for HTA 2.0. Washing and staining were performed using a

GeneChip Fluidics 450. Scanning was performed with a GeneChip Scanner 3000. These data were deposited in the Gene Expression Omnibus under accession GSE85033.

Validation Sample Processing

We applied a quality control pipeline [19] to all CEL files generated by the HTA 2.0. All validation samples passed processing quality control, which included an inspection of spatial artifacts, MA plots, probe distributions, and sample comparison boxplots. We summarized transcript intensities using robust multi-array analysis (RMA) [20]. We determined batch normalization was unnecessary after a guided principal components analysis (gPCA) using sample processing date and array plate ID as potential batch effect confounders [21]. Lastly, we collapsed HTA2.0 transcripts into gene level measurements using the `collapseRows()` function with the "maxmean" method from the R package WGCNA [22]. We used the pd.hta.2.0 platform design file (version 3.12.1) and the Bioconductor package "hta20sttranscriptcluster.db" (version 8.3.1) to map manufacturer transcript IDs to genes. We performed all preprocessing steps using R version 3.2.3.

Western Blotting

Prior to sodium dodecyl sulfate polyacrylamide gel electrophoresis, protein sample concentration was determined using a Pierce BCA Protein Assay Kit (Thermo Scientific). Protein samples were prepared with 1X Laemmli sample buffer (50 mM Tris pH 6.8, 0.02% w/v bromophenol blue, 2% w/v SDS, 10% v/v glycerol, 1% v/v beta-mercaptoethanol, 12.5 mM EDTA) and 50 µg of tumor protein. Volumes were normalized with RIPA buffer including the protease/phosphatase inhibitors described above. SDS-PAGE was performed using a 4-15% Mini-PROTEAN TGX gel (Bio-Rad) for 1 hour at 120V. The samples were then transferred to a nitrocellulose membrane for 2 hours and 45 minutes at 400 mA in cold transfer buffer (384 mM glycine, 50 mM Tris, 20% methanol, 0.005% w/v sodium dodecyl sulfate. Following this,

the blots were then blocked in 5% w/v BSA or 5% w/v nonfat dry milk in Tris-buffered saline (137 mM NaCl, 2.7 mM KCl, 19 mM Tris, 0.05% v/v Tween 20, pH 7.4) for 25 minutes. Immunoblotting was performed with the following antibodies and conditions (vendor, species, diluent, dilution, incubation time, incubation temperature): anti-NF1 D7R7 (Cell Signaling, rabbit, 2% BSA, 1:1000, overnight, 4°C), anti-tubulin B-1-2-5 (Santa Cruz, mouse, 2% milk, 1:10000, 1 hour, RT), anti-EGFR D38B1 (Cell Signaling, rabbit, 2% milk, 1:1000-1:2000, 1h, RT), p-ERK ½ (p44/42 MAPK) #9101 (Cell Signaling, rabbit, 2% BSA, 1:2000, overnight, 4°C), SUZ12 D39F6 #3737 (Cell Signaling, rabbit, 2% milk, 1:1000, overnight, 4°C). Anti-NF1 D7R7 was a kind gift from Cell Signaling Technologies, Inc.

The binding of the primary antibodies was detected by incubation with secondary antibodies goat anti-rabbit HRP 1:20000 or goat anti-mouse HRP 1:10000 (Jackson Immunoresearch Laboratories Inc.) at room temperature in 2% milk in TBST and detection of HRP activity using Pierce ECL Western Blotting substrate (Thermo Scientific), or in the case of *NF1*, SuperSignal West Femto Maximum Sensitivity Substrate (Thermo Scientific). The chemiluminescent signal was captured with MED-B medical x-ray film (Med X Ray Company Inc.). Between primary antibodies, the membrane was stripped twice for 10 minutes at room temperature using a mild stripping buffer containing 1.5% w/v glycine, 0.1% w/v SDS, 1% v/v Tween 20 at pH 2.2 (Abcam). One sample was eliminated due to low yield, and apparent degradation as determined by western blotting (all proteins examined were undetectable with the exception of tubulin, not shown). Densitometry was performed using Li-COR Image Studio Lite 5.0. Briefly, intensity measurements for *NF1* and tubulin were taken using equally-sized regions for all bands. The background was subtracted using the local median intensity from the left and right borders (size=2) of each measurement region. *NF1* values were divided by tubulin intensity to adjust for protein loading. All measurement ratios were then normalized by dividing values by the “U87+PI” measurement for each blot, respectively.

Reproducibility of Computational Analyses

We provide software with a permissive open source license to reproduce all computational analyses [23]. Ensuring a stable compute environment, we performed all analyses in a Docker image [24]. This image and source code can be used to freely confirm, modify, and build upon this work.

RESULTS:

Classifier performance

Using 5-fold cross validation across a parameter sweep, we identified optimal hyperparameters at alpha = 0.15 and L1 mixing = 0.1 (Supplementary Figure S1). To assess model performance, we performed 100 random initializations of five-fold cross-validation. These models had mean test area under the receiver operating characteristic curve (AUROC) of 0.77 (95% Quantiles: 0.53 – 0.95) and a mean train AUROC of 0.997 (95% Quantile: 0.98 – 1.00) (Supplementary Figure S2). We repeated this procedure after TDM transformation (Supplementary Figure S3) and achieved comparable results with alpha = 0.15 and l1 mixing = 0.1 (mean test AUROC = 0.77, 95% Quantiles: 0.51 – 0.96; mean train AUROC = 0.998, 95% Quantiles: 0.99 – 1.00) (Figure 1). Because the validation set was measured by microarray, we used the classifier trained on TDM transformed data to construct our ensemble classifier.

Identification and characterization of NF1 deficient glioblastoma tumor samples

We characterized NF1 protein concentrations as well as other molecules involved in RAS signaling in the 12 GBM samples (Figure 2A). Two samples (CB2, 3HQ) had no apparent NF1 protein. Eight other samples had similar or less NF1 signal than the U87-MG NF1-low control (H5M, LNA, YXL, VVN, R7K, TRM, UNY, W31). Two samples (PBH, RIW) had equal or greater NF1 than the positive control, U87-MG + proteasome inhibitors (preventing *NF1* degradation). We also observed variable EGFR content in these

261 samples, with non-existent to low levels (3HQ, YXL, R7K), or medium to large EGFR signal (CB2, H5M,
262 PBH, LNA, YXL, VVN, RIW, TRM, UNY, W31). All GBM samples had high concentrations of phospho-
263 ERK1/2 signal relative to cell line controls. Samples with increased phospho-ERK1/2 may have greater
264 Ras pathway activation. This can be attributed to multiple factors, including increased EGFR expression
265 and/or NF1 inactivation.

266 Our ensemble classifier predicted four samples to have NF1 inactivation (CB2, UNY, R7K, and 3HQ)
267 and eight samples to be NF1 wildtype (W31, TRM, PBH, VVN, LNA, RIW, H5M, and YXL) (Figure 2B).
268 Because two samples, (CB2 and H5M) were measured on both western blots (Figure 2C), we used the
269 mean of their NF1 protein level across both experiments (Figure 2D).

270 One of the samples predicted to be NF1 inactive contains detectable NF1 protein (R7K), suggesting
271 that this sample may have NF1 inactivation not detectable by assaying protein, have a different
272 alteration that phenocopies NF1 loss, or is incorrectly predicted by the classifier. Conversely, there are
273 three samples predicted to be NF1 wildtype that have low or undetectable protein (YXL, VVN, W31),
274 which either indicates unknown elements that confound the detection of some NF1 dysregulated
275 tumors or a classification error.

276

277 *Highly Contributing Genes*

278 We observed several genes that consistently contributed to the ensemble classifier performance
279 (Figure 3). Since we applied several classifiers to the validation set as an ensemble, we took the sum of
280 all classifier's gene weights across all 500 iterations to define these consistently contributing genes.
281 Expression of genes such as *TXNIP, ARRDC4, ISPD, C10orf107*, and *DUSP18* appear to be predictive of
282 intact NF1 signaling. Among the list of genes that appear to be expressed in tumors with loss of NF1
283 function are *QPRT, ATF5, HUS1B, PEG10, HMGA2, RSL1D1, and NRG1*. A full list of positive and negative

284 weight genes that were two standard deviations beyond the gene weight distribution is provided in
285 Supplementary Table S2.
286 We also performed over-representation analysis of the most influential genes in the classifier to
287 identify gene ontology (GO) sets and pathways that may be predictive of NF1 status [25–28]
288 (Supplemental Table S3). For high-weight genes predictive of intact NF1 signaling, we observed GO sets
289 involved in plasma membrane-localized proteins (GO:0005886, GO:0071944, GO:0016324) and
290 homeostasis (GO:0048871, GO:0001659, GO:0048873, GO:0031224), among others. Annotated
291 pathways associated with genes from this dataset include hematopoietic stem cell differentiation,
292 thyroid cancer, voltage-gated potassium channels, and RHO GTPase functional pathways.
293 For high-weight genes predictive of NF1 loss of function, we observed GO sets related to cellular
294 adhesion (GO:0007155, GO:0098742), negative regulation of signaling (GO:0009968, GO:0023507,
295 GO:0010648), and nervous system development (GO:0051962, GO0007416, GO: 0050808), among
296 others. These genes were also enriched for elements of the phototransduction cascade and thyroxine
297 production pathways.
298
299 **DISCUSSION:**
300 A machine learning classifier, based on gene expression data, can capture signal associated with the
301 inactivation of a tumor suppressor. Our classifier is able to detect subtle downstream changes in gene
302 expression as a result of the tumor responding to NF1 loss of function. This finding supports using mRNA
303 as a summary measurement capable of capturing system-wide responses to molecular events beyond
304 transcription factor alterations. Machine learning has been applied to gene expression in a variety of
305 studies with various goals [29–33]. In a similar study, Guinney *et al.* trained a classifier to model RAS
306 activity in colorectal cancer and demonstrated its clinical utility by predicting response to MEK inhibitors
307 and anti-EGFR based treatments [34]. With a wealth of signal embedded in gene expression and a

rapidly growing library of datasets, the performance of machine learning models is likely to rapidly improve. An increase in performance leads to more reliable clinical applications that would potentially predict the effectiveness of pathway-specific targeted therapies.

While our classifier was able to predict NF1 inactivation status to an extent, its performance is far from being clinically actionable. A major difficulty in developing a reliable classifier in this case is contamination in gold standard positives and negatives. While we aim to detect NF1 inactivation events, our gold standard positives can only include samples with known *NF1* mutation status. Conversely, we expect that negative samples (about 90% of the data) are also contaminated with NF1 inactivated samples due to protein loss and other mechanisms. We cannot determine scenarios where NF1 is inactivated beyond mutation at scale in the TCGA data. Another challenge with the construction of classifiers from such data is overfitting. Even after hyperparameter optimization we observed substantial overfitting (Figure 2), which has also been observed in competitions (see, for example, supplementary figure S2 of Noren *et al*. 2016 [35] in which the best performing algorithms also overfit). Finally with a small number of positive examples the model performance is unstable, which demonstrates high variability in gold standard samples used to train the model [36]. We employed ensemble classification to mitigate this issue. In summary, our results are promising but these challenges are substantial and significant work remains to reach a robust classifier with clinical utility.

The performance of the classifier appears to be impacted by many *NF1* related genes. For example, genes such as *TXNIP* and *ARRDC4*, which are both indicative of lactic acidosis, correlate with better clinical outcomes, and contribute to predicting tumors with intact NF1 signaling [37]. We also observed transcripts that are more highly expressed in brain tissue than either other normal tissue (*ISPD, C10orf107*), or more highly expressed in normal brain tissue than glioma (*EPHA5*) [38–40]. *DUSP18* contributes to the prediction of *NF1* wildtype status and is a negative regulator of ERK phosphorylation, possibly by regulating *SHP2* phosphorylation [41]. Over-representation analysis of these data

highlighted changes in potassium channel expression. It was previously demonstrated that *NF1* wild-type Schwann cells have altered K+ channel activity as compared to *NF1*$^{-/-}$ Schwann cells suggesting that this may be one factor by which *NF1* mutant and wild-type cells can be distinguished [42].

Regarding prediction of NF1 inactivated tumors, we observed several genes that have been linked to cancer such as *QPRT*, which is highly expressed in malignant pheochromocytomas as compared to benign; *RSL1D1* (CSIG), which stabilizes *c-myc* in hepatocellular carcinoma; *PPEF*, which is highly expressed in astrocytic gliomas as compared to normal brain tissue [43–45]; and *PEG10*, a poor prognostic marker and regulator of proliferation, migration, and invasion in several tumor types [46–48]. We also observed *ATF5,* a gene for which expression in malignant glioma is correlated with poor survival [49]. Knockdown of *ATF5* in GBM cells causes cell death *in vitro* and *in vivo* [50]. Analysis of genes that contribute to the prediction of *NF1* inactivation yielded several GO terms related to neural development. It is well established that loss of *NF1* can result in abnormal neural development and/or tumorigenesis [14,51,52]. We also observed genes associated with the mesodermal commitment pathway, components of which are linked to the epithelial to mesenchymal transition in human cancer cells [53–55]. Analysis of this pathway may be informative in identifying tumors with *NF1* loss because mesenchymal GBMs are enriched for tumors with *NF1* loss [56].

Our ensemble classifier was able to robustly detect the samples with the highest and lowest NF1 protein concentrations, but it struggled with samples of intermediate NF1 concentrations. This could be a result of an enrichment of mechanisms causing NF1 inactivation beyond protein abundance, an overrepresentation of mesenchymal tumors in NF1 inactivated samples contaminating dataset splits [56], poor classifier generalizability, or incomplete data transformation between RNAseq and microarray data. Because training and testing performance were similar between transformed and non-transformed data (see Figure 1 and Supplementary Fig S2) we don't anticipate performance to be impacted much by platform differences or classifier generalizability. Nevertheless, we demonstrated the

ability of system-wide gene expression measurements to capture downstream consequences of a complex biological mechanism that would otherwise require several different types of data acquisition to capture.

CONCLUSIONS:

A machine learning classifier for transcriptomic data was able to detect signal associated with the inactivation of *NF1*, a tumor suppressor gene. The gene is an important regulator of the oncogene *RAS* and is inactivated frequently in GBM and in other tumors. The measurement of NF1 inactivity cannot be comprehensively captured by any single genomic characterization such as targeted sequencing or fluorescence in situ hybridization. This difficulty arises from diverse and complex biological mechanisms that inactivate the tumor suppressor in a variety of ways. However, we demonstrated that measuring system-wide RNA can capture subtle downstream changes that occur in response to NF1 inactivation. Improving classification performance is required before transitioning such a model into clinical use, but our method could be used to characterize cell lines or patient-derived xenograft (PDX) models with inactive NF1. Eventually, with more data and improved classification, we expect machine-learning models constructed on system-wide transcriptomics will translate into clinically relevant predictions that will guide targeted therapy.

DECLARATIONS:

Ethics approval and consent to participate

The Dartmouth-Hitchcock Medical Center declared IRB review and approval is not required since the study does not meet the regulatory definition of human subjects.

Consent for publication

Not Applicable

Availability of data and materials

All source code is available under a permissive open source license in the nf1_inactivation GitHub repository, https://github.com/greenelab/nf1_inactivation. We also provide a docker image to replicate the computational environment at https://hub.docker.com/r/gregway/nf1_inactivation/. Additionally, all validation data is available under Gene Expression Omnibus accession number GSE85033.

Competing interests

The authors declare no competing interests.

Funding

This work was funded by the Genomics and Computational Biology PhD Program at The University of Pennsylvania to GPW, The Gordon and Betty Moore Foundation GBMF4552 to CSG, NINDS R01 NS095411 to YS and CSG, Children's Tumor Foundation Young Investigator Award 2014-01-12 to RJA, a Nancy P. Shea Trust grant to YS, a Prouty Pilot Grant from the Friends of the Norris Cotton Cancer Center to YS, a Synergy grant to YS, CSG and CF funded by NIH NCATS UL1 TR001086 to The Dartmouth Center for Clinical and Translational Science, NCI Cancer Center Support Grant P30 CA023108 to the Dartmouth-Hitchcock Norris Cotton Cancer Center. RJA is an Albert J. Ryan Fellow.

Authors' contributions

GPW built, analyzed, and interpreted the classifier, generated the figures, created all source code, and wrote the manuscript. RJA performed all experiments, interpreted the classifier, and wrote the

manuscript. SJB interpreted the results and was a major contributor to the manuscript. CEF was a major contributor to the study design and was a major contributor to the manuscript. YS designed the study, interpreted the results, and wrote the manuscript. CSG designed the study, interpreted the results, and wrote the manuscript. All authors read and approved the final manuscript.

Acknowledgements

This work was supported by the MMC BioBank, a core facility of the Maine Medical Center Research Institute, and the Dartmouth Genomics Shared Resource, a core facility of the Norris Cotton Cancer Center.

FIGURES:

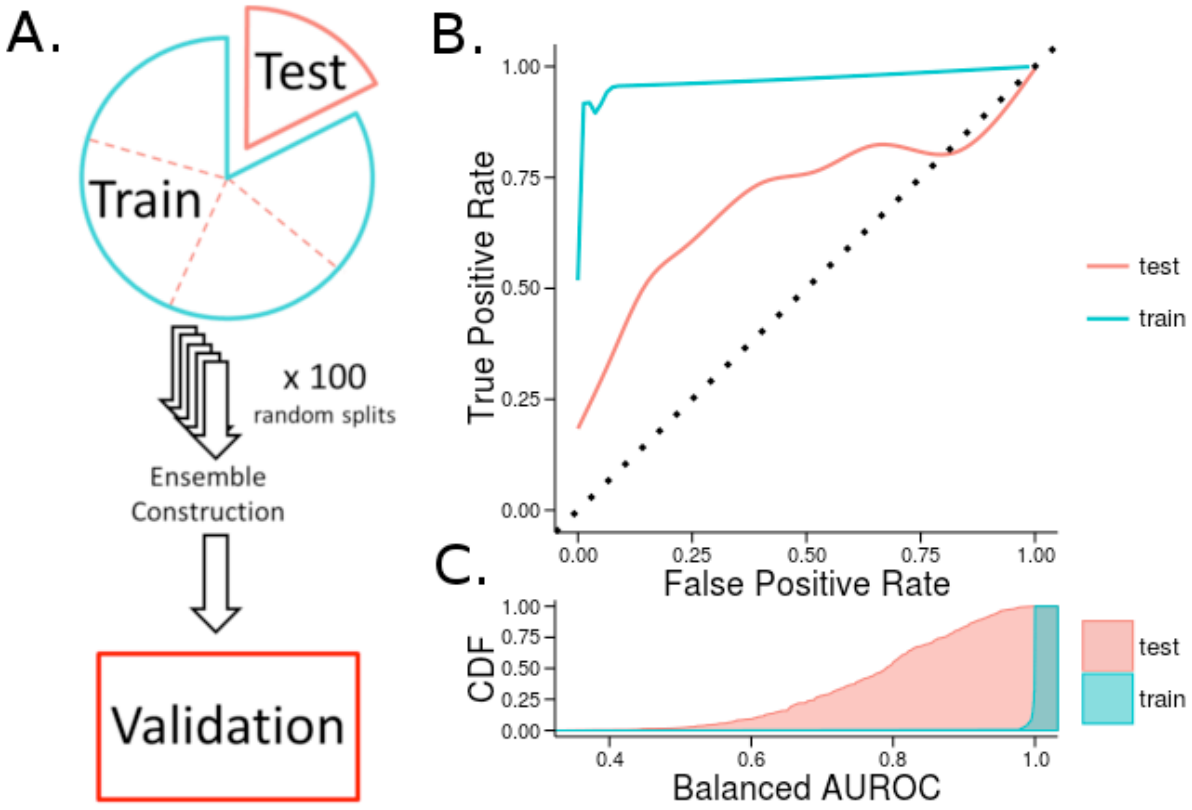

Figure 1: *Logistic regression classifier with elastic net penalty training and testing errors over 100 iterations for Training Distribution Matching (TDM) transformation of The Cancer Genome Atlas Glioblastoma RNAseq data.* (A) Schematic describing the terms used for training, testing, and validating our model. We applied 5-fold cross validation to the full dataset which consists of training and testing splits in each fold. The model is then applied as an ensemble classifier on a set of in-house samples (validation set) (B) Receiver operating characteristic (ROC) curve and shows the average training and testing performance of 5-fold cross validation. (C) The cumulative density of area under the ROC curve (AUROC) balanced by 0-1 class for training and testing partitions.

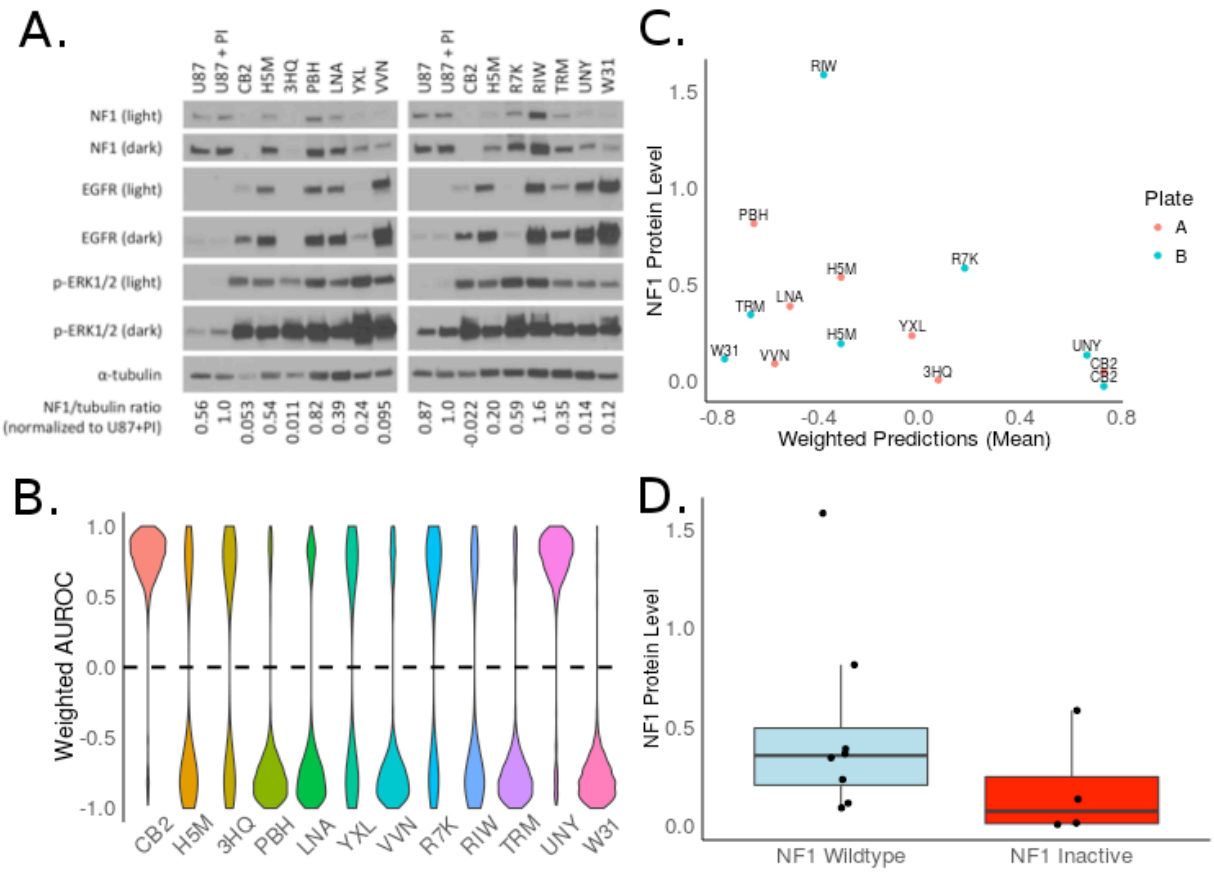

Figure 2: *Performance of our classifier on a validation set.* (A) Two distinct western blots for each of our twelve samples. The controls are U87-MG, an *NF1* WT glioblastoma cell line that exhibits proteasomal degradation of the *NF1* protein. U87+PI are U87-MG cells are treated with the proteasome inhibitors (PI) MG-132 and bortezomib to block proteasome-mediated degradation of *NF1*. We used the NF1/tubulin ratio normalized to U87+PI as our NF1 protein level estimate. (B) Our ensemble classifier performance weighted by test set AUROC where a negative number indicates NF1 wildtype and a positive number is predictive of NF1 inactivation. (C) We quantify protein against U87+PI and provide the mean of the weighted predictions. (D) Based on weighted predictions, we show the abundance of NF1 protein compared to U87+PI.

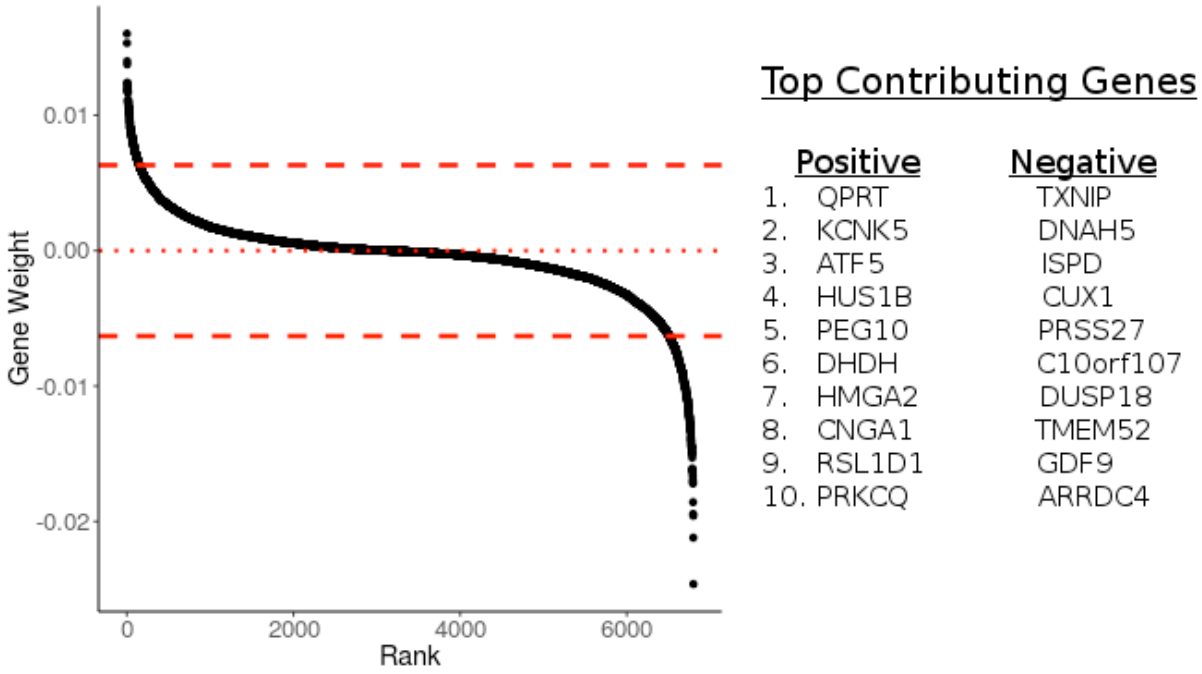

Figure 3: *Genes that contribute to the classifier performance.* Genes are shown ranked by their weighted contribution to the ensemble classifier. Weights are scaled to unit norm. The top 10 positive and top 10 negative contributing high weight genes are given on the right.

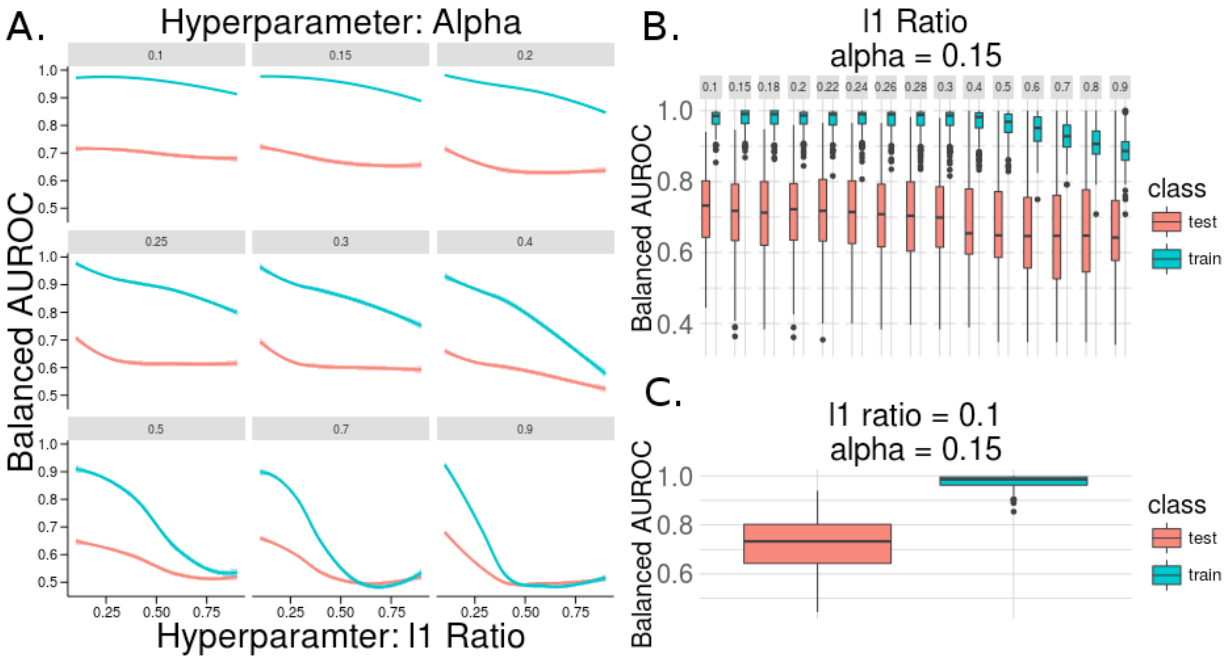

Supplementary Figure S1: *Non-transformed RNAseq results of The Cancer Genome Atlas Glioblastoma parameter sweep for stochastic gradient descent logistic classifiers with elastic net penalty.* (A) Training and testing area under the receiver operating characteristic curve (AUROC) balanced by class is given for each parameter tested. All accuracies are presented following 5-fold cross validation after 50 random initializations. (B) The l1 mixing parameter with the optimal alpha and (C) the classifier performance across all random starts for the best hyperparameters.

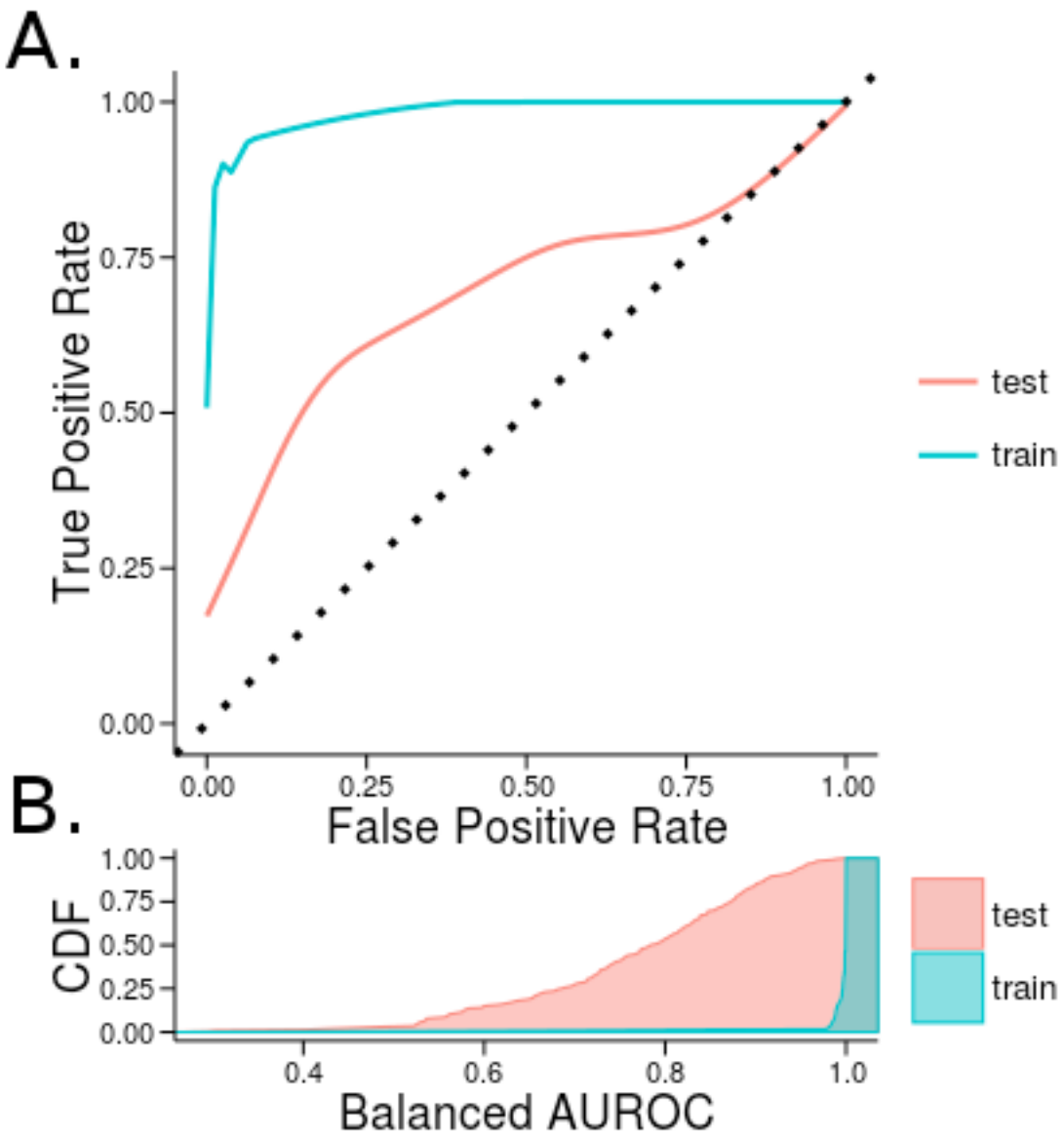

482

483 Supplementary Figure S2: *Logistic regression classifier with elastic net penalty training and testing errors*

484 *over 100 iterations for non-transformed The Cancer Genome Atlas Glioblastoma RNAseq data.* (A)

485 Receiver operating characteristic (ROC) curve and shows the average training and testing performance

486 of 5-fold cross validation over 100 random initializations. (B) The cumulative density of area under the

487 ROC curve (AUROC) balanced by 0-1 class for training and testing partitions.

488

489

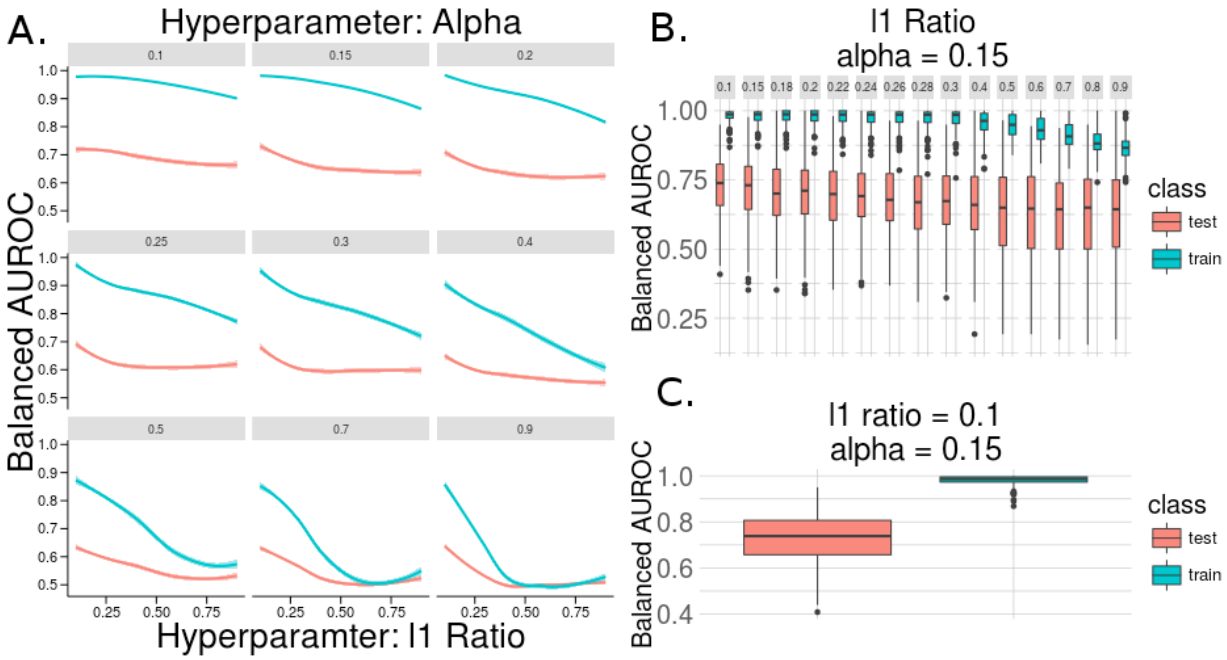

Supplementary Figure S3: *Training Distribution Matching (TDM) transformation of RNAseq results of The Cancer Genome Atlas Glioblastoma parameter sweep for stochastic gradient descent logistic classifier with elastic net penalty.* (A) Training and testing area under the receiver operating characteristic curve (AUROC) balanced by class is given for each parameter tested. All accuracies are presented following 5-fold cross validation after 100 random initializations. (B) The l1 mixing parameter with the optimal alpha and (C) the classifier performance across all random starts for the best hyperparameters.

REFERENCES:

1. Martin GA, Viskoohil D, Bollag G, McCabe PC, Crosier WJ, Haubruck H, et al. The GAP-related domain of the neurofibromatosis type 1 gene product interacts with ras p21. Cell. 1990;63:843–9.

2. Xu G, O'Connell P, Viskochil D, Cawthon R, Robertson M, Culver M, et al. The neurofibromatosis type 1 gene encodes a protein related to GAP. Cell. 1990;62:599–608.

3. Boyd KP, Korf BR, Theos A. Neurofibromatosis type 1. J. Am. Acad. Dermatol. 2009;61:1–14.

4. Dogra B, Rana K. Facial plexiform neurofibromatosis: A surgical challenge. Indian Dermatol. Online J. 2013;4:195.

5. Evans DGR, Baser M, McGaughran J, Sharif S, Howard E, Moran A. Malignant peripheral nerve sheath tumours in neurofibromatosis 1. J. Med. Genet. 2002;39:311–4.

6. Rad E, Tee AR. Neurofibromatosis type 1: Fundamental insights into cell signalling and cancer. Semin. Cell Dev. Biol. 2016;52:39–46.

7. Ratner N, Miller SJ. A RASopathy gene commonly mutated in cancer: the neurofibromatosis type 1 tumour suppressor. Nat. Rev. Cancer. 2015;15:290–301.

8. Wood M, Rawe M, Johansson G, Pang S, Soderquist RS, Patel AV, et al. Discovery of a Small Molecule Targeting IRA2 Deletion in Budding Yeast and Neurofibromin Loss in Malignant Peripheral Nerve Sheath Tumor Cells. Mol. Cancer Ther. 2011;10:1740–50.

9. Allaway RJ, Fischer DA, de Abreu FB, Gardner TB, Gordon SR, Barth RJ, et al. Genomic characterization of patient-derived xenograft models established from fine needle aspirate biopsies of a primary pancreatic ductal adenocarcinoma and from patient-matched metastatic sites. Oncotarget. 2016;7:17087–102.

10. McGillicuddy LT, Fromm JA, Hollstein PE, Kubek S, Beroukhim R, De Raedt T, et al. Proteasomal and Genetic Inactivation of the NF1 Tumor Suppressor in Gliomagenesis. Cancer Cell. 2009;16:44–54.

11. Subramanian S, Thayanithy V, West RB, Lee C-H, Beck AH, Zhu S, et al. Genome-wide transcriptome analyses reveal p53 inactivation mediated loss of miR-34a expression in malignant peripheral nerve sheath tumours. J. Pathol. 2010;220:58–70.

12. Wallace MR, Andersen LB, Saulino AM, Gregory PE, Glover TW, Collins FS. A de novo Alu insertion results in neurofibromatosis type 1. Nature. 1991;353:864–6.

13. Skuse GR, Cappione AJ, Sowden M, Metheny LJ, Smith HC. The Neurofibromatosis Type I Messenger RNA Undergoes Base-Modification RNA Editing. Nucleic Acids Res. 1996;24:478–86.

14. Cichowski K, Jacks T. NF1 tumor suppressor gene function: narrowing the GAP. Cell. 2001;104:593–604.

15. UCSC Xena [Internet]. Available from: http://xena.ucsc.edu/

16. Brennan CW, Verhaak RGW, McKenna A, Campos B, Noushmehr H, Salama SR, et al. The Somatic Genomic Landscape of Glioblastoma. Cell. 2013;155:462–77.

17. Thompson JA, Tan J, Greene CS. Cross-platform normalization of microarray and RNA-seq data for machine learning applications. PeerJ. 2016;4:e1621.

18. Pedregosa F, Varoquaux G, Gramfort A, Michel V, Thirion B, Grisel O, et al. Scikit-learn: Machine Learning in Python. CoRR. 2012;

19. Carvalho BS, Irizarry RA. A framework for oligonucleotide microarray preprocessing. Bioinforma. Oxf. Engl. 2010;26:2363–7.

539 20. Irizarry RA, Bolstad BM, Collin F, Cope LM, Hobbs B, Speed TP. Summaries of Affymetrix GeneChip
540 probe level data. Nucleic Acids Res. 2003;31:e15.

541 21. Reese SE, Archer KJ, Therneau TM, Atkinson EJ, Vachon CM, de Andrade M, et al. A new statistic for
542 identifying batch effects in high-throughput genomic data that uses guided principal component
543 analysis. Bioinformatics. 2013;29:2877–83.

544 22. Miller JA, Cai C, Langfelder P, Geschwind DH, Kurian SM, Salomon DR, et al. Strategies for
545 aggregating gene expression data: The collapseRows R function. BMC Bioinformatics. 2011;12:322.

546 23. Greg Way. nf1_inactivation: Pre-Release. 2016 [cited 2016 Aug 1]; Available from:
547 http://dx.doi.org/10.5281/zenodo.58864

548 24. Boettiger C. An introduction to Docker for reproducible research. ACM SIGOPS Oper. Syst. Rev.
549 2015;49:71–9.

550 25. Kamburov A, Wierling C, Lehrach H, Herwig R. ConsensusPathDB--a database for integrating human
551 functional interaction networks. Nucleic Acids Res. 2009;37:D623–8.

552 26. Kamburov A, Stelzl U, Lehrach H, Herwig R. The ConsensusPathDB interaction database: 2013
553 update. Nucleic Acids Res. 2013;41:D793–800.

554 27. Ashburner M, Ball CA, Blake JA, Botstein D, Butler H, Cherry JM, et al. Gene Ontology: tool for the
555 unification of biology. Nat. Genet. 2000;25:25–9.

556 28. The Gene Ontology Consortium. Gene Ontology Consortium: going forward. Nucleic Acids Res.
557 2015;43:D1049–56.

558 29. Molla M, Waddell M, Page D, Shavlik J. Using Machine Learning to Design and Interpret Gene-
559 Expression Microarrays. AI Mag. 2004;25:23–44.

560 30. Bastani M, Vos L, Asgarian N, Deschenes J, Graham K, Mackey J, et al. A Machine Learned Classifier
561 That Uses Gene Expression Data to Accurately Predict Estrogen Receptor Status. Rogers S, editor. PLoS
562 ONE. 2013;8:e82144.

563 31. Pirooznia M, Yang JY, Yang MQ, Deng Y. A comparative study of different machine learning methods
564 on microarray gene expression data. BMC Genomics. 2008;9:S13.

565 32. Chou W-C, Ma Q, Yang S, Cao S, Klingeman DM, Brown SD, et al. Analysis of strand-specific RNA-seq
566 data using machine learning reveals the structures of transcription units in Clostridium thermocellum.
567 Nucleic Acids Res. 2015;43:e67–e67.

568 33. Tan J, Hammond JH, Hogan DA, Greene CS. ADAGE-Based Integration of Publicly Available
569 *Pseudomonas aeruginosa* Gene Expression Data with Denoising Autoencoders Illuminates Microbe-Host
570 Interactions. Gilbert JA, editor. mSystems. 2016;1:e00025–15.

571 34. Guinney J, Ferte C, Dry J, McEwen R, Manceau G, Kao K, et al. Modeling RAS Phenotype in Colorectal
572 Cancer Uncovers Novel Molecular Traits of RAS Dependency and Improves Prediction of Response to
573 Targeted Agents in Patients. Clin. Cancer Res. 2014;20:265–72.

574 35. Noren DP, Long BL, Norel R, Rrhissorrakrai K, Hess K, Hu CW, et al. A Crowdsourcing Approach to
575 Developing and Assessing Prediction Algorithms for AML Prognosis. Tan K, editor. PLOS Comput. Biol.
576 2016;12:e1004890.

577 36. Yu B. Stability. Bernoulli. 2013;19:1484–500.

578 37. Chen JL-Y, Merl D, Peterson CW, Wu J, Liu PY, Yin H, et al. Lactic Acidosis Triggers Starvation
579 Response with Paradoxical Induction of TXNIP through MondoA. Gibson G, editor. PLoS Genet.
580 2010;6:e1001093.

581 38. Willer T, Lee H, Lommel M, Yoshida-Moriguchi T, de Bernabe DBV, Venzke D, et al. ISPD loss-of-
582 function mutations disrupt dystroglycan O-mannosylation and cause Walker-Warburg syndrome. Nat.
583 Genet. 2012;44:575–80.

584 39. Thierry-Mieg D, Thierry-Mieg J. AceView: a comprehensive cDNA-supported gene and transcripts
585 annotation. Genome Biol. 2006;7 Suppl 1:S12.1–14.

586 40. Almog N, Ma L, Raychowdhury R, Schwager C, Erber R, Short S, et al. Transcriptional Switch of
587 Dormant Tumors to Fast-Growing Angiogenic Phenotype. Cancer Res. 2009;69:836–44.

588 41. Sacco F, Boldt K, Calderone A, Panni S, Paoluzi S, Castagnoli L, et al. Combining affinity proteomics
589 and network context to identify new phosphatase substrates and adapters in growth pathways. Front.
590 Genet. [Internet]. 2014 [cited 2016 Aug 1];5. Available from:
591 http://journal.frontiersin.org/article/10.3389/fgene.2014.00115/abstract

592 42. Xu Y, Chiamvimonvat N, Vázquez AE, Akunuru S, Ratner N, Yamoah EN. Gene-targeted deletion of
593 neurofibromin enhances the expression of a transient outward K+ current in Schwann cells: a protein
594 kinase A-mediated mechanism. J. Neurosci. Off. J. Soc. Neurosci. 2002;22:9194–202.

595 43. Thouënnon E, Elkahloun AG, Guillemot J, Gimenez-Roqueplo A-P, Bertherat J, Pierre A, et al.
596 Identification of Potential Gene Markers and Insights into the Pathophysiology of Pheochromocytoma
597 Malignancy. J. Clin. Endocrinol. Metab. 2007;92:4865–72.

598 44. Cheng Q, Yuan F, Lu F, Zhang B, Chen T, Chen X, et al. CSIG promotes hepatocellular carcinoma
599 proliferation by activating c-MYC expression. Oncotarget. 2015;6:4733–44.

600 45. Bageritz J, Puccio L, Piro RM, Hovestadt V, Phillips E, Pankert T, et al. Stem cell characteristics in
601 glioblastoma are maintained by the ecto-nucleotidase E-NPP1. Cell Death Differ. 2014;21:929–40.

602 46. Deng X, Hu Y, Ding Q, Han R, Guo Q, Qin J, et al. PEG10 plays a crucial role in human lung cancer
603 proliferation, progression, prognosis and metastasis. Oncol. Rep. 2014;32:2159–67.

604 47. Li C-M, Margolin AA, Salas M, Memeo L, Mansukhani M, Hibshoosh H, et al. PEG10 is a c-MYC target
605 gene in cancer cells. Cancer Res. 2006;66:665–72.

606 48. Akamatsu S, Wyatt AW, Lin D, Lysakowski S, Zhang F, Kim S, et al. The Placental Gene PEG10
607 Promotes Progression of Neuroendocrine Prostate Cancer. Cell Rep. 2015;12:922–36.

608 49. Sheng Z, Li L, Zhu LJ, Smith TW, Demers A, Ross AH, et al. A genome-wide RNA interference screen
609 reveals an essential CREB3L2-ATF5-MCL1 survival pathway in malignant glioma with therapeutic
610 implications. Nat. Med. 2010;16:671–7.

611 50. Greene LA, Lee HY, Angelastro JM. The transcription factor ATF5: role in neurodevelopment and
612 neural tumors. J. Neurochem. 2009;108:11–22.

613 51. Zhu Y, Romero MI, Ghosh P, Ye Z, Charnay P, Rushing EJ, et al. Ablation of NF1 function in neurons
614 induces abnormal development of cerebral cortex and reactive gliosis in the brain. Genes Dev.
615 2001;15:859–76.

616 52. Joseph NM, Mosher JT, Buchstaller J, Snider P, McKeever PE, Lim M, et al. The Loss of Nf1 Transiently
617 Promotes Self-Renewal but Not Tumorigenesis by Neural Crest Stem Cells. Cancer Cell. 2008;13:129–40.

618 53. Morishita A, Zaidi MR, Mitoro A, Sankarasharma D, Szabolcs M, Okada Y, et al. HMGA2 is a driver of
619 tumor metastasis. Cancer Res. 2013;73:4289–99.

620 54. de Boeck M, Cui C, Mulder AA, Jost CR, Ikeno S, ten Dijke P. Smad6 determines BMP-regulated
621 invasive behaviour of breast cancer cells in a zebrafish xenograft model. Sci. Rep. 2016;6:24968.

622 55. Salomonis N, Mshel016, Cirillo E, Hanspers K, Kutmon M. Mesodermal Commitment Pathway (Homo
623 sapiens). http://www.wikipathways.org/index.php/Pathway:WP2857.

624 56. Verhaak RGW, Hoadley KA, Purdom E, Wang V, Qi Y, Wilkerson MD, et al. Integrated genomic
625 analysis identifies clinically relevant subtypes of glioblastoma characterized by abnormalities in PDGFRA,
626 IDH1, EGFR, and NF1. Cancer Cell. 2010;17:98–110.

627